Cell Stem Cell, volume 11

Supplemental Information

The Par Complex and Integrins Direct Asymmetric Cell Division in Adult Intestinal Stem Cells

Spyros Goulas, Ryan Conder, and Juergen A. Knoblich

Supplemental Figures

Suppl. Figure 1, related to Figure 1

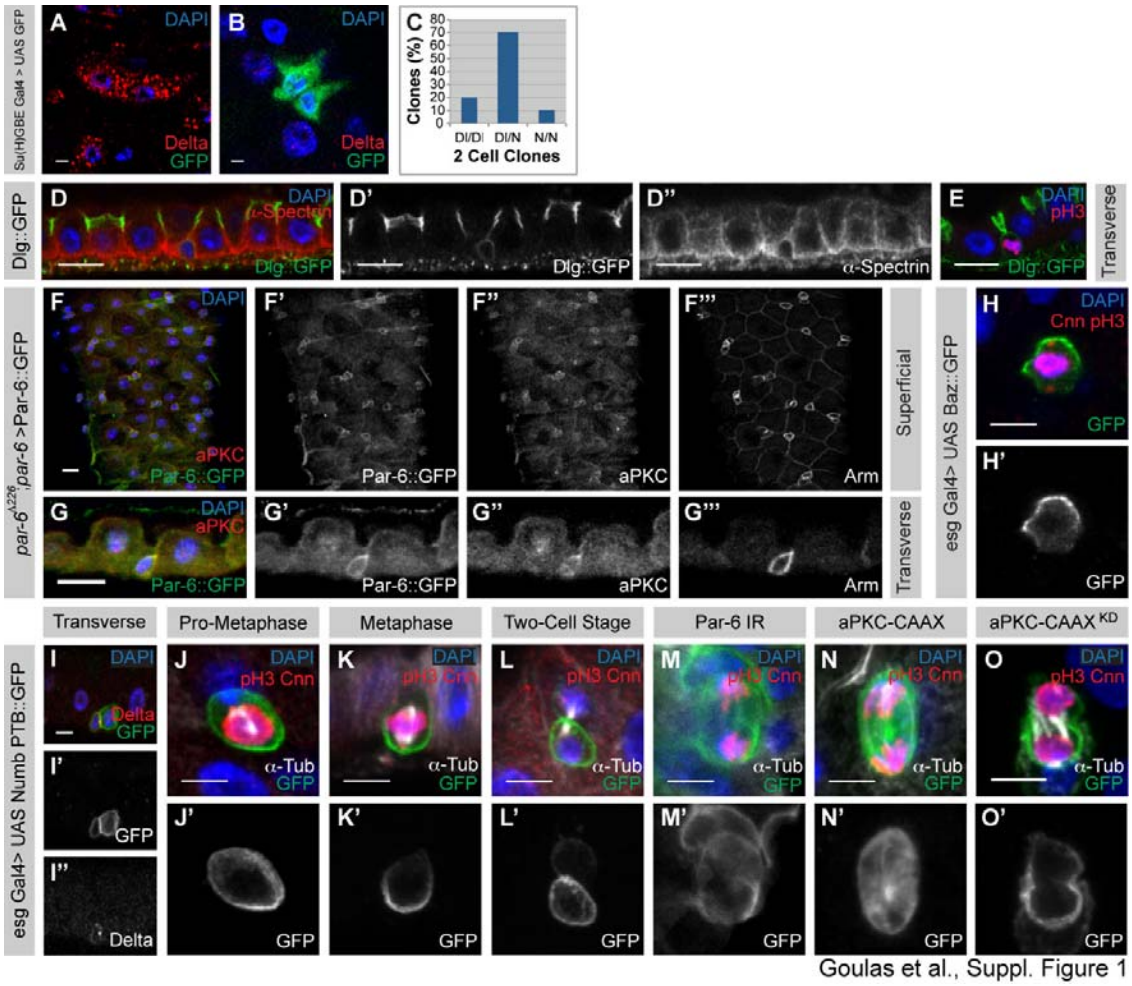

Goulas et al., Suppl. Figure 1

Suppl. Figure 2, related to Figure 2

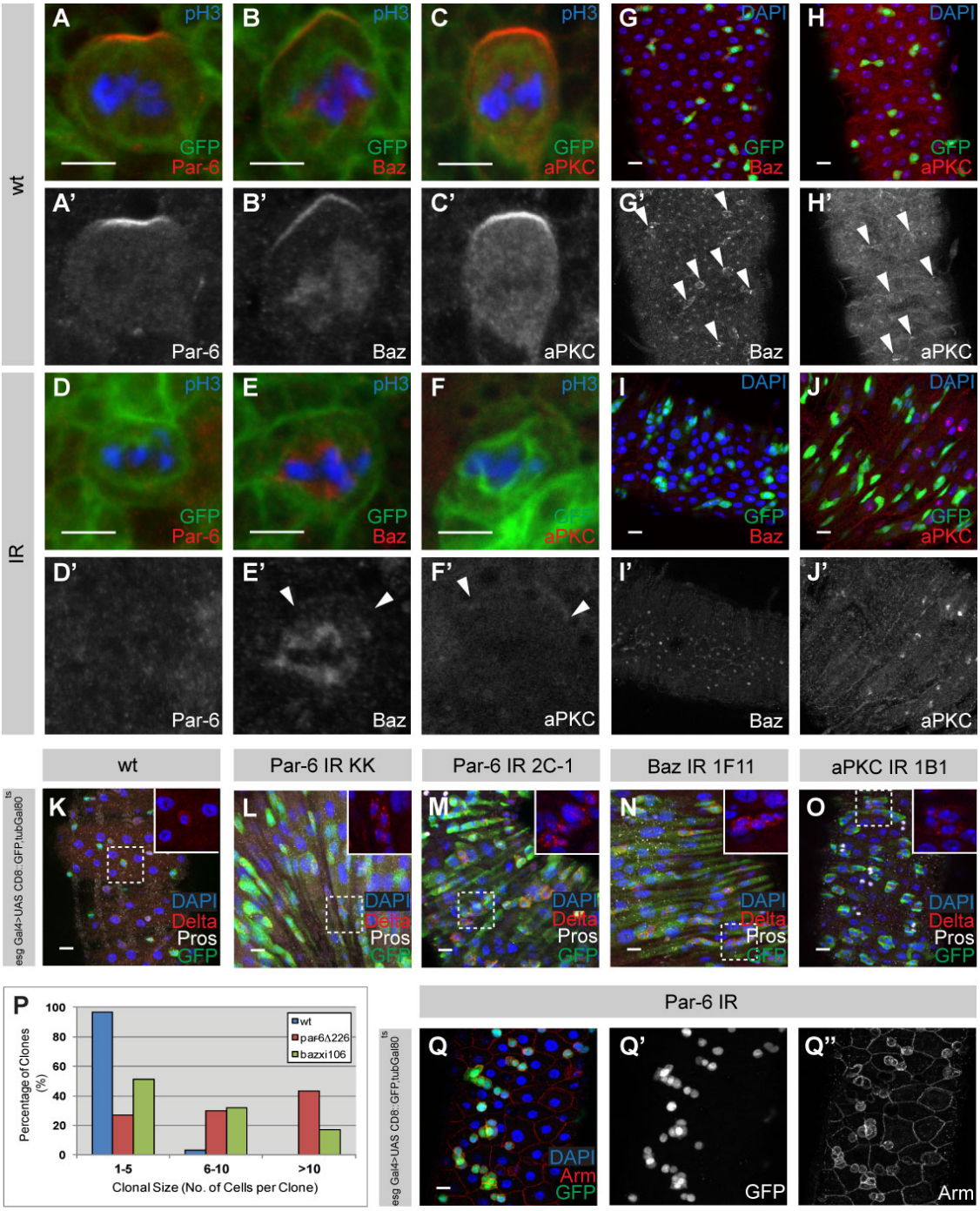

Goulas et al., Suppl. Figure 2

Suppl. Figure 3, related to Figure 3

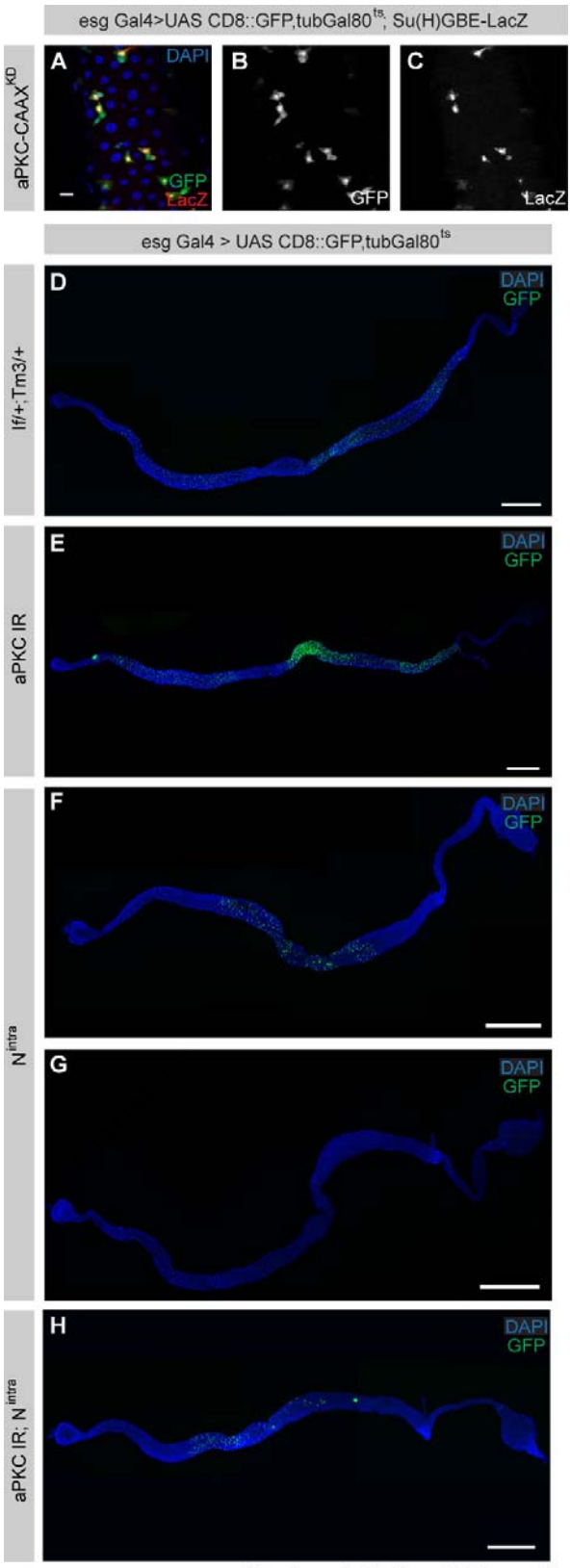

Goulas et al., Suppl. Figure 3

Suppl. Figure 4, related to Figure 4

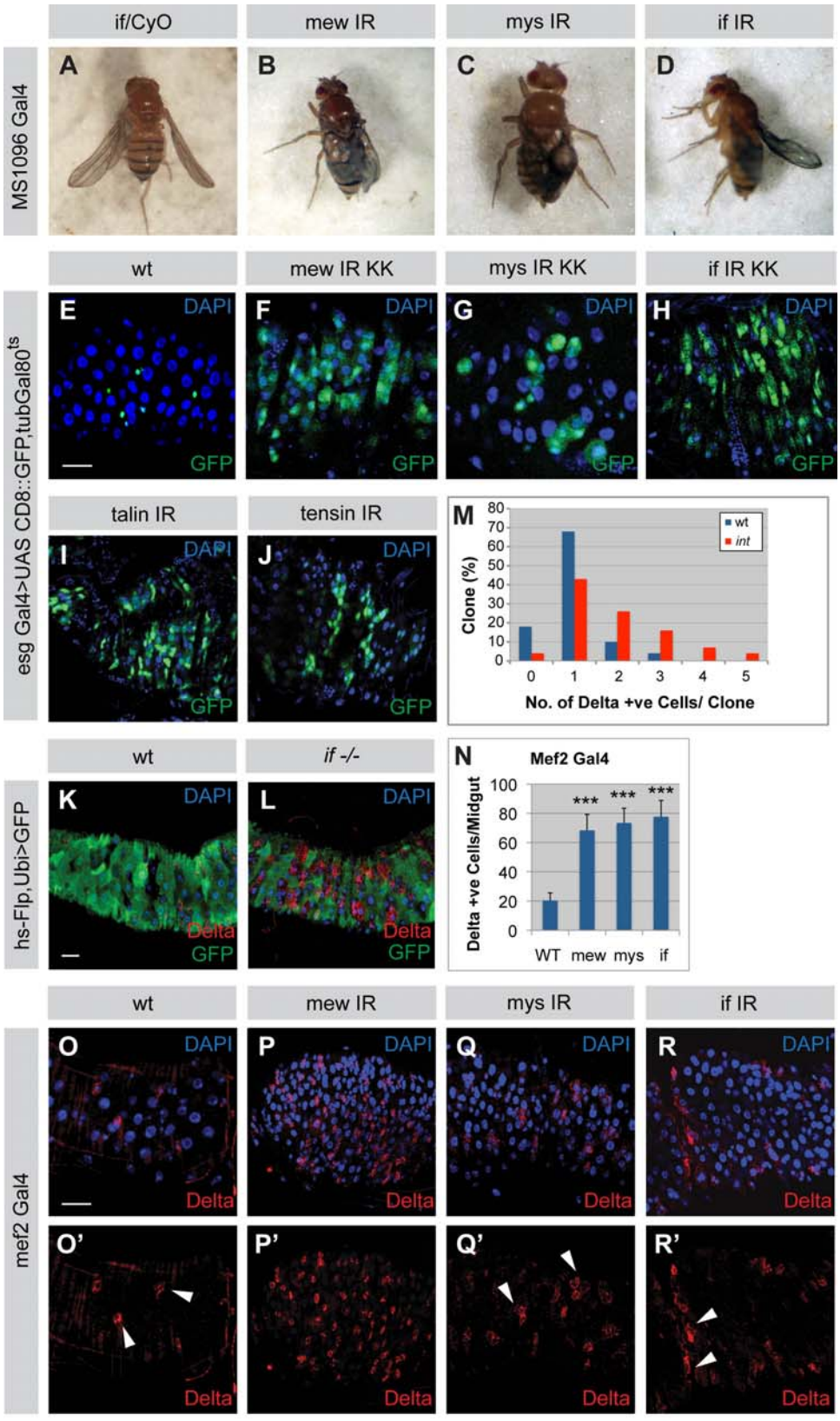

Goulas et al., Suppl. Figure 4

Suppl. Figure 5, related to Figure 5

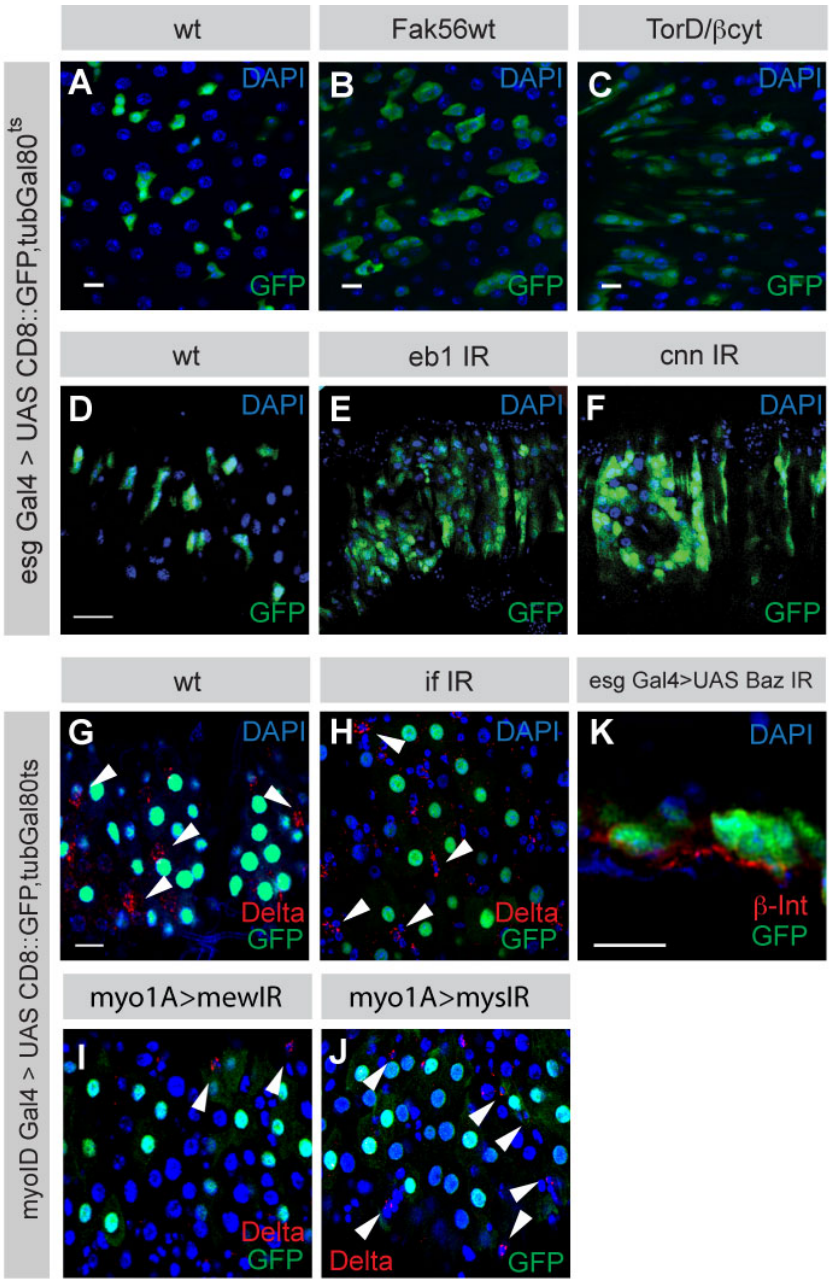

Goulas et al., Suppl. Figure 5

Supplemental Figure Legends

Figure S1 related to Figure 1.

The adult *Drosophila* intestinal tract is a polarized epithelial monolayer in which the Par complex is apical and aPKC is active during mitosis.

(A,B) Lineage analysis examples of Dl/Dl (A, red) and N/N doublets (B, green). 2 Cell clone analysis (C, n=10).

(D,E) Tranverse view of the polarized *Drosophila* intestinal epithelium. α-Spectrin (D, red) is expressed along the lateral domain of the ECs while the septate junction marker Dlg (green) is expressed in the apico-lateral domain of ECs (D) and weakly cortical in mitotic (red) ISCs (E). α-Spectrin localization differed further anterior within the posterior midgut with stronger apico-lateral staining in ECs similar to what has been described previously (Baumann, 2001).

(F-H) aPKC and Baz localize asymmetrically with Par-6. Superficial (F) and transverse (G) view of intestinal tract. aPKC (red) co-localises with Par-6::GFP (green) in ISCs whereas Arm is localized uniformly around the cortex and basolaterally in ECs. Baz::GFP (H, green) localises asymmetrically to the apical cortex during mitosis (pH3, red) in ISCs.

(I-O) aPKC activity dependent asymmetric localization of Numb PTB::GFP (green) during mitosis in ISCs. Numb PTB::GFP is symmetric during interphase (I) and polarises at pro-metaphase (J) to become asymmetric later in mitotic ISCs (K, L). Numb PTB::GFP localization is perturbed when the Par complex is mislocalized upon Par-6 IR knockdown (M) to the cell cortex and the ectopic activity of aPKC with aPKC-CAAX (N) to the cytoplasm , yet not with a kinase dead version of aPKC-CAAX^{KD} (O).

Scale bar = 10μm (D-G), = 5μm (A, B, H-O).

Figure S2 related to Figure 2.

Knockdown efficiency of members of the Par complex in larval neuroblasts and adult midgut together with secondary/ternary Par complex RNAi lines and mutant verification of knockdown phenotypes.

(A-F) In larval neuroblasts (green, CD8::GFP), Par-6 (A, red), Baz (B, red) and aPKC (C, red) localize asymmetrically in mitosis (blue, pH3). Targeted RNAi knockdown of Par-6 (D, red), Baz (E, red) and aPKC (F, red) in the larval neuroblasts. Arrowheads show the residual proteins after knockdown (E, F). Note the non-specific staining around the nucleus (E).

(G-J**)** In adult midguts, Baz (G, red) and aPKC (H, red) is enriched in the apical domain of ISCs and EBs (arrowheads). RNAi knockdown of Baz (I, red) and aPKC (J, red). Note the non-specific staining in nucleus of ECs.

(K-O) Secondary/ternary Par complex RNAi knockdowns result in ectopic ISCs and EBs. Secondary Par-6 RNAi (L) (KK line, VDRC) and customized RNAi knockdowns of Par-6 (M), Baz (N) and aPKC (O) (Mummery-Widmer et al., 2009) cause increase in *esg* positive cells (green) with some forming Delta positive ISC clusters (insets) in comparison to the wild-type (K).

(P) Quantification of clonal size between mutant clones of $par\text{-}6^{\Delta 226}$ (n=30 clones) and baz^{xi106} (n=53 clones) in comparison to wt (n=31 clones) 4 days after heatshock induction.

(Q) Knockdown of Par-6 in ISC/EBs does not perturb epithelial polarity. The basolateral epithelial marker Arm (Q'') is unaffected upon the knockdown of Par-6 using *esg* GAL4 (Q').

Scale bar = 5μm (A-F), = 10μm (G-O, Q).

Figure S3 related to Figure 3.

aPKC kinase activity acts on Notch signalling and Notch is epistatic to the Par complex.

(A-C) aPKC-$CAAX^{KD}$ causes mild effects on Notch activity. Merged image (A), GFP channel alone (B) and Su(H)GBE-LacZ channel alone (C).

(D-H) Single plane image reconstruction of entire guts demonstrating Notch is epistatic to the Par complex. Internal control gut (D, n=7 guts) showing distribution of *esg* positive ISC/EB cells (green) in midgut. aPKC RNAi knockdown (E, n=9/11 guts) leads to an increase in *esg* positive cells. Variance of $Notch^{intra}$ phenotypes (F, G) ranging from weak with a small reduction (F, n=2/6 guts) to elimination (G, n=4/6 guts) of *esg* positive cells. Note that the anterior domain of the anterior midgut and posterior domain of the posterior midgut are both

reduced (C). Expression of aPKC IR and Notch^{intra} reduces the severity of aPKC knockdown phenotype (H, n=7/8 guts).

Scale bar = 10μm (A-C), = 500μm (D-H)

Figure S4 related to Figure 4.

Knockdown efficiency of Integrin RNAi lines and confirmation of RNAi phenotypes with secondary RNAi lines and mutants.

(A-D) Wing blistering Integrin RNAi phenotypes. Cyo wings (A) seen in *MS1096* Gal4 driver (0% blisters seen in 25 flies). Knockdown with RNAi against *mew* (B), *mys* (C) and *if* (D) results in wing blistering, characteristic of loss of Integrins (100% blistering in all of 25 flies in each).

(E-H) Secondary Integrin IR lines. Clusters of *esg* positive (green) cells in *mew* (F), *mys* (G) and *if* (H) RNAi knockdowns (KK lines, VDCR) in comparison to wild-type (E).

(I, J) Knockdown of Talin (I) and Tensin (J) leads to *esg* positive cell clusters (green).

(K-M) Integrin mutant phenotypes. Negatively-marked GFP (green) Flp-out clones in FRT line alone (K) with ISCs marked by Delta (red) and if^{B2} mutant (L) showing ectopic Delta positive cells. Quantification (M) of Delta positive cells per clone represented as a percentage of total clones between wild-type and with *integrin* alleles combined. Difference between expected Delta positive cell possibilities (0-2) and unexpected (>3). $P<0.01$.

(N-R) Confocal Z projections of knockdown of either α or β Integrin subunit with the *mef2* Gal4 driver, expressed in the surrounding musculature, results in ectopic Delta positive cells in the midgut. Clusters of Delta positive cells (arrowheads) in *mew* (P), *mys* (Q) and *if* (R) RNAi knockdowns in comparison to wild-type (O). Quantification of *mef2* Gal4 Integrin knockdowns (N). $P<0.01$.

Scale bar = 10μm

Figure S5 related to Figure 5.

Integrin-mediated adhesion and components of spindle orientation apparatus are required for the limiting of ISC self renewal.

(A-C) Overexpression of the dominant negative Integrin adhesion constructs FAK^{56wt} (B) and Tor^{D}/β_{cyt} (C) leads to proliferation defects in comparison to wild-type (A).

(D-F) RNAi knockdown of spindle machinery leads to the overproliferation of ISCs and EBs. RNAi knockdown of EB1 (E) and Cnn (F) by the *esg* Gal4 driver leads to *esg* postive clustering of ISCs in comparison to the wild-type (D).

(G-J) Knockdown of Integrins (*if*, H, *mew*, I and *mys*, J) in EC cells with *Myo1A* Gal4 driver does not affect the number of Delta positive cells (G).

(K) Integrin localization is not affected upon knockdown of Baz.

Scale bar =10μm

Supplemental Experimental Procedures

Fly Strains

yw; esg Gal4 (Goto and Hayashi, 1999), esg Gal4,UAS CD8::GFP,tubGal80^{ts} (Micchelli and Perrimon, 2006), esg Gal4,UAS CD8::GFP,tubGal80^{ts}/CyO; Su(H)GBE-LacZ/Tm6B, MS1096 Gal4; if/CyO,wg-LacZ (Gift from A. Martinez-Arias), mef2 Gal4 (Gift from F. Schnorrer), myo1A Gal4, UAS CD8::GFP,tubGal80^{ts} (Jiang et al., 2009), UAS Dicer2; 1407 Gal4,UAS CD8::GFP/CyO (Neumuller et al., 2011), tubGal80^{ts}; delta Gal4 (Zeng et al., 2010), Su(H)GBE Gal4, UAS-CD8::GFP (Zeng et al., 2010), UASp Baz::GFP (Benton and Johnston, 2003), esg Gal4/CyO;UAS Baz::GFP/Tm6B, UAS NumbPTB::GFP (Roegiers et al., 2001), esg Gal4,UAS NumbPTB::GFP/CyO, UAS aPKC-CAAXwt (Sotillos et al., 2004), UAS aPKC-CAAXwt/CyO; tubGal80ts/Tm6b, Dlg::GFP (Buszczak et al., 2007) (obtained from Flytrap), Vkg::GFP (Morin et al., 2001), obtained from Dlytrap), UAS N^{intra} MH3 (gift from Sarah Bray), UAS Tor^{D}/β_{cyt} (Palmer et al., 1999), UAS FAK^{56wt} (Martin-Bermudo and Brown, 1999), UAS aPKCRNAi (GD and KK line, VDRC; 1B1 line, (Mummery-Widmer et al., 2009)), UAS BazRNAi (GD line, VDRC; 1F 11 line, (Mummery-Widmer et al., 2009)), UAS Par-6RNAi (GD and KK line, VDRC; 2C-1 line, (Mummery-Widmer et al., 2009)), tubGAL80ts/CyO;UAS Par-6RNAi/Tm6b, UAS mewRNAi (GD and KK line, VDRC), UAS ifRNAi (GD and KK line, VDRC), UAS mysRNAi (GD and KK line, VDRC), UAS eb1RNAi (GD line, VDRC), UAS cnnRNAi (GD line, VDRC), UAS talinRNAi (GD line, VDRC), UAS tensin RNAi (GD line, VDRC), par-6$^{\Delta 226}$;par-6>par-6::GFP (Wirtz-Peitz et al., 2008), hsflp;; act >CD2> Gal4, UAS-GFP (Buttitta et al., 2007), hsflp; Act25FRT-y-FRT-Gal4, UAS-lacZN for clonal analysis, *mys*^{XG43} FRT101 (Leptin et al., 1989), *mew*^{P13} FRT101 (Prokop et al., 1998), *if*^{B2} FRT19A (Brown, 1994), *par-6*$^{\Delta 226}$ FRT9-2/Fm7KrGFP (Petronczki and Knoblich, 2001), *baz*^{xi106} FRT9-2/Fm7; hsflp/CyO , 1xGFP FRT9-2hsflp (Muller and Wieschaus, 1996)Ubi-GFP FRT19A and 101 (Bloomington) .

Immunohistochemistry

Primary antibodies used: mouse anti-Armadillo (DSHB, 1:100), mouse anti-Discs Large (DSHB, 1:100), mouse anti-Prospero (DSHB, 1:5), mouse anti-Delta (DSHB, 1:100), mouse anti-βPS Integrin (DSHB, 1:200), mouse anti-α Tubulin (Sigma, 1:500), mouse anti-GFP

(Roche, 1:2000), rabbit anti-phospho-Histone H3 (Ser10) (Upstate, 1:1000), chicken anti-GFP (Abcam, 1:1000), chicken anti-β-Galactosidase (Abcam, 1:1000), rabbit anti-Centrosomin (gift from Thom Kaufman, 1:500), mouse anti-γ Tubulin (Sigma, 1:1000), rabbit anti-Laminin β-1 (Abcam, 1:1000), rabbit anti-aPKC (Santa Cruz, 1:500 in brains, 1:300 in midguts), rabbit anti-Par-6 (1:100) (Petronczki and Knoblich, 2001), rabbit anti-Baz (1:200) (Wirtz-Peitz et al., 2008), rabbit and rat anti-Baz (Wodarz et al., 1999) and rabbit and guinea pig anti-Pros serum using the peptide sequence (Vaessin et al., 1991), DMDSLASPSHSDMMLLDKDDVLDEDDDDDC, 1:1200.

Secondary antibodies used: goat anti-chicken Alexa-488 (Invitrogen, 1:500), goat anti-mouse Alexa-488 (Invitrogen, 1:500), goat anti-mouse Alexa-568 (Invitrogen, 1:500), goat anti-mouse Alexa-647 (Invitrogen, 1:500), goat anti-rabbit Alexa-488 (Invitrogen, 1:500), goat anti-rabbit Alexa-568 (Invitrogen, 1:500), goat anti-rabbit Alexa-647 (Invitrogen, 1:500), goat anti-guinea pig Alexa-647 (Invitrogen, 1:500), goat anti-rat Alexa 568 (Invitrogen, 1:500), goat anti-rat Alexa 647 (Invitrogen, 1:500).

Female adult intestinal tracts were dissected in PBS and fixed immediately in 4% PFA in PBS for 15-20min. Fix was washed with PBS and transferred to blocking solution (2% NGS (Sigma) in 0.1% PBS/Triton X-100) for 1hr at RT or overnight at 4 degrees. After blocking, specimens were incubated with the primary antibodies diluted in blocking solution for 3hrs at RT or overnight at 4 degrees. Primary antibodies were rinsed twice in 0.1% PBS/Tx and washed twice for at least 15min each before adding the secondary antibodies for 1hr at RT or overnight at 4 degrees. Secondary was rinsed and washed with 0.1% PBS/Tx and transferred to PBS and exchanged with 50% PBS/glycerol before being mounted on slides with Vector Shield mounting medium with DAPI (Vector Laboratories). Alternatively, dissections were done in Grace's Insect Medium and fixed and stained as described previously (Lin et al., 2008) and mounted on Vector Shield.

TARGET system and Temperature Shifting

Temporal and Regional Gene Expression Targeting (TARGET) system was used for temporal and spatial control of transgene expression in adult flies. Crosses were set up either at 18 degrees or 22 degrees and adult flies, 1-3 day after eclosion (AE), were transferred to

new vials with fresh food and kept in 29 degree incubators for approximately 10 days unless specified and were dissected and stained.

Two-Cell Pair Analysis

Cells were marked with Delta, identifying the ISC and *Su(H) GBE* Gal4 , identifying the EB. In all cases images were acquired by confocal sections through the midgut and upon analysis "cell-pairs" were confidently identified by the "adjoining" shape provided by the two signals.

Clonal Analysis

Clones were induced by heat shock in a 37 degree water bath of adult flies 1-3 days AE. This was done in three steps whereby two 30 min heat shock were performed with a 30 min intermission (resting period) between consecutive heat shocks. Flies after heat shock, were transferred to new vials with fresh food and kept at 25 degrees for 4-5days and were dissected and stained.

2 cell clonal analysis was performed as described above whereby clones were positively labelled by GFP under the *Act* Gal4 driver after heatshock, which was also labelled by Su(H)GBE-LacZ to identify EBs. This was then dissected 1 day after heatshock.

In positively marked LacZ clones, the heat shock results in mosaic flipping out of the stop cassette allowing *Gal4* expression and the positive labelling of mitotic clones with an Nls-LacZ. 104 and 102 cell clones were counted in the wt and UAS-aPKC-CAAX overexpression through confocal-Z stacks, from which 43 and 46 clones were single cells, respectively. Single cell clones that were either mature ECs or ee cells were removed from the count as the heat shock likely flipped out in these cells rather than in the ISCs.

Negatively marked clones were induced and visualised in a similar manner, except that the heat shock results in the mosaic flipping out a GFP cassette resulting in negatively marked cells within a wild-type/heterozygous background.

Delta Positive Cell Counts

All cell counts were performed in a defined region between the hindgut and the middle midgut.

Analysis of Asymmetric Protein Localization During ISC divisions

To determine the localization of proteins during mitosis, we dissected and stained for the required markers/proteins. Typically, confocal Z stacks of the whole cell were taken with a 40x Oil Immersion Objective at 4x zoom with 0.7μm optical sections. To determine apico-basal polarity of the cell, we used Cnn to label centrosomes together with the position of the surrounding musculature/basement membrane to distinguish the basal side from the apical side within the confocal Z-stack. Maximum projections of the Z-stacks were taken for the images. Images were then rotated along the axis of division.

Calculation of Spindle Orientation

To calculate the angle of ISC divisions, midguts were dissected and stained for GFP, phospho-H3, Cnn or gamma-tubulin and Laminin. Confocal Z-stacks of whole cells were taken with 0.75μm optical sections and reconstituted in 3D using IMARIS software and movies were made from the 3D images. Using Laminin to label the basement membrane, the angle of division was determined through bisecting the chromatin and centrosomes of late mitotic cells and measuring the angle between the two vectors. Significance calculated by Wilcoxon rank sum test.

Supplemental References

Baumann, O. (2001). Posterior midgut epithelial cells differ in their organization of the membrane skeleton from other drosophila epithelia. Exp Cell Res *270*, 176-187.

Benton, R., and Johnston, D. S. (2003). Drosophila PAR-1 and 14-3-3 inhibit Bazooka/PAR-3 to establish complementary cortical domains in polarized cells. Cell *115*, 691-704.

Brown, N. H. (1994). Null mutations in the alpha PS2 and beta PS integrin subunit genes have distinct phenotypes. Development *120*, 1221-1231.

Buszczak, M., Paterno, S., Lighthouse, D., Bachman, J., Planck, J., Owen, S., Skora, A. D., Nystul, T. G., Ohlstein, B., Allen, A., Wilhelm, J. E., Murphy, T. D., Levis, R. W., Matunis, E., Srivali, N., Hoskins, R. A., and Spradling, A. C. (2007). The carnegie protein trap library: a versatile tool for Drosophila developmental studies. Genetics *175*, 1505-1531.

Buttitta, L. A., Katzaroff, A. J., Perez, C. L., de la Cruz, A., and Edgar, B. A. (2007). A Double-Assurance Mechanism Controls Cell Cycle Exit upon Terminal Differentiation in Drosophila. Dev Cell *12*, 631-643.

Goto, S., and Hayashi, S. (1999). Proximal to distal cell communication in the Drosophila leg provides a basis for an intercalary mechanism of limb patterning. Development *126*, 3407-3413.

Jiang, H., Patel, P. H., Kohlmaier, A., Grenley, M. O., McEwen, D. G., and Edgar, B. A. (2009). Cytokine/Jak/Stat signaling mediates regeneration and homeostasis in the Drosophila midgut. Cell *137*, 1343-1355.

Leptin, M., Bogaert, T., Lehmann, R., and Wilcox, M. (1989). The function of PS integrins during Drosophila embryogenesis. Cell *56*, 401-408.

Lin, G., Xu, N., and Xi, R. (2008). Paracrine Wingless signalling controls self-renewal of Drosophila intestinal stem cells. Nature *455*, 1119-1123.

Martin-Bermudo, M. D., and Brown, N. H. (1999). Uncoupling integrin adhesion and signaling: the betaPS cytoplasmic domain is sufficient to regulate gene expression in the Drosophila embryo. Genes Dev *13*, 729-739.

Micchelli, C. A., and Perrimon, N. (2006). Evidence that stem cells reside in the adult Drosophila midgut epithelium. Nature *439*, 475-479.

Morin, X., Daneman, R., Zavortink, M., and Chia, W. (2001). A protein trap strategy to detect GFP-tagged proteins expressed from their endogenous loci in Drosophila. Proc Natl Acad Sci U S A *98*, 15050-15055.

Muller, H. A., and Wieschaus, E. (1996). armadillo, bazooka, and stardust are critical for early stages in formation of the zonula adherens and maintenance of the polarized blastoderm epithelium in Drosophila. J Cell Biol *134*, 149-163.

Mummery-Widmer, J. L., Yamazaki, M., Stoeger, T., Novatchkova, M., Bhalerao, S., Chen, D., Dietzl, G., Dickson, B. J., and Knoblich, J. A. (2009). Genome-wide analysis of Notch signalling in Drosophila by transgenic RNAi. Nature *458*, 987-992.

Neumuller, R. A., Richter, C., Fischer, A., Novatchkova, M., Neumuller, K. G., and Knoblich, J. A. (2011). Genome-wide analysis of self-renewal in Drosophila neural stem cells by transgenic RNAi. Cell Stem Cell *8*, 580-593.

Palmer, R. H., Fessler, L. I., Edeen, P. T., Madigan, S. J., McKeown, M., and Hunter, T. (1999). DFak56 is a novel Drosophila melanogaster focal adhesion kinase. J Biol Chem *274*, 35621-35629.

Petronczki, M., and Knoblich, J. A. (2001). DmPAR-6 directs epithelial polarity and asymmetric cell division of neuroblasts in Drosophila. Nat Cell Biol *3*, 43-49.

Prokop, A., Martin-Bermudo, M. D., Bate, M., and Brown, N. H. (1998). Absence of PS integrins or laminin A affects extracellular adhesion, but not intracellular assembly, of hemiadherens and neuromuscular junctions in Drosophila embryos. Dev Biol *196*, 58-76.

Roegiers, F., Younger-Shepherd, S., Jan, L. Y., and Jan, Y. N. (2001). Two types of asymmetric divisions in the Drosophila sensory organ precursor cell lineage. Nat Cell Biol *3*, 58-67.

Sotillos, S., Diaz-Meco, M. T., Caminero, E., Moscat, J., and Campuzano, S. (2004). DaPKC-dependent phosphorylation of Crumbs is required for epithelial cell polarity in Drosophila. J Cell Biol *166*, 549-557.

Vaessin, H., Grell, E., Wolff, E., Bier, E., Jan, L. Y., and Jan, Y. N. (1991). prospero is expressed in neuronal precursors and encodes a nuclear protein that is involved in the control of axonal outgrowth in Drosophila. Cell *67*, 941-953.

Wirtz-Peitz, F., Nishimura, T., and Knoblich, J. A. (2008). Linking cell cycle to asymmetric division: Aurora-A phosphorylates the Par complex to regulate Numb localization. Cell *135*, 161-173.

Wodarz, A., Ramrath, A., Kuchinke, U., and Knust, E. (1999). Bazooka provides an apical cue for Inscuteable localization in Drosophila neuroblasts. Nature *402*, 544-547.

Zeng, X., Chauhan, C., and Hou, S. X. (2010). Characterization of midgut stem cell- and enteroblast-specific Gal4 lines in drosophila. Genesis *48*, 607-611.